Inorganic Chemistry

Article

pubs.acs.org/IC

Diffusion-Controlled Formation of Ti_2O_3 during Spark-Plasma Synthesis

I. Veremchuk,*[,†] I. Antonyshyn,[†] C. Candolfi,[†] X. Feng,[†,‡] U. Burkhardt,[†] M. Baitinger,[†] J.-T. Zhao,[‡] and Yu. Grin[†]

[†]Max-Planck-Institut für Chemische Physik fester Stoffe, Nöthnitzer Straβe 40, 01187 Dresden, Germany

[‡]Key Laboratory of Transparent Opto-Functional Inorganic Materials of Chinese Academy of Science, Shanghai Institute of Ceramics, Shanghai 200050, China

ABSTRACT: The spark-plasma-sintering (SPS) technique has successfully been applied for the single-step direct synthesis of Ti_2O_3 from a mixture of powders of rutile/anatase with titanium. The components react by diffusion through the grain boundaries, forming several intermediate phases locally. A single-phase material of titanium(III) oxide is obtained in compact bulk form after 180 min of SPS treatment at 1473 K. The electrical and thermal transport properties of such a SPS-prepared material measured in the temperature range between 300 and 800 K reflect the known semiconductor-to-metal transition above 400 K. The observed metallic-like electrical and thermal conductivity above this temperature is in good agreement with previously reported results. A maximum of the thermoelectric figure-of-merit ZT = 0.04 is achieved at 350 K.

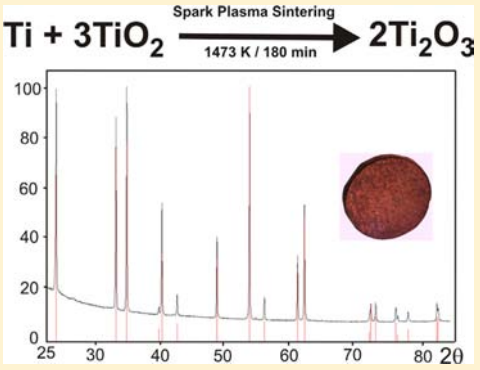

INTRODUCTION

An important task of contemporary science is focused on finding new, fast, reproducible, and energy-efficient synthetic routes for bulk quantity production of new and known functional materials. In addition, for practical use, these materials are often required to be manufactured in specified shapes. Spark-plasma sintering (SPS) is a one of the advanced densification techniques developed over the last decades that may fulfill these requirements. As one of the main features of SPS, the millisecond-pulsed direct current (*dc*) passes directly through the die, as well as through the powder green body. Other significant features of the SPS method are a high heating rate, the application of pressure, and the effect of the *dc*.[1,2]

Recently, the development and production of new thermoelectric materials have evolved into a central goal of application- and basic knowledge-driven research programs in many countries. Through such intensified research, many materials with the high thermoelectric figure-of-merit ZT have been developed. However, these materials are often of limited use, in particular for operation at high temperatures (above 800 K), because of decomposition and possible vaporization of the constituents. In addition, these materials should be comprised of inexpensive, readily abundant elements of low toxicity. Oxides and borides are promising classes of candidates within this field of high-temperature thermoelectrics. Consequently, the study of oxide materials for potential use in thermoelectrics is rapidly progressing. Some key findings are *n*-type high-mobility In−Sn−O mixed oxides,[3] hopping conduction in $CaMnO_3$-based perovskites,[4] $SrTiO_3$-based perovskites with heavy effective mass of electrons,[5] composites of the layer-structured homologous series $(ZnO)_mIn_2O_3$,[6] and aluminum-doped ZnO as one of the best *n*-type oxide-based thermoelectrics so far.[7] Typical ZT values of the n-type materials lie between 0.3 and 0.4, which are lower than those for practically used thermoelectric materials. An important performance can be expected for *p*-type oxides. Extensive studies on cobalt-based layered oxides were triggered by the discovery of the large thermopower of $NaCo_2O_4$.[8] The family of cobalt oxides including $Ca_3Co_4O_9$[9] and $Bi_2Sr_2Co_2O_y$[10] exhibits ZT values close to 1. A layered structure seems to be one of the key features for a good thermoelectric performance. Yet, one of the major drawbacks of oxide materials stems from the difficulty to obtain both *n*- and *p*-type materials from the same "mother" compound.

The titanium oxides raised considerable interest, specifically with respect to thermoelectricity. The Ti−O system is characterized by the formation of many phases with complex crystal structures. The first detailed investigation of the phase diagram was performed within the range of 0−67 atom % of oxygen;[11] complete information about the Ti−O system is available in a previous review.[12] Interesting intermediate compounds in this system are Magnéli phases Ti_nO_{2n-1}[11,13] followed by Ti_2O_3.[14] In particular, Magnéli phases are interesting because of their special building principle, resulting in structural complexity and unusual electrical properties.[15] Just recently, a high dimensionless figure-of-merit ZT of 1.6 has been reported for *p*-type $TiO_{1.1}$, rendering this oxide as an attractive material for thermoelectric applications.[16]

Received: December 10, 2012
Published: March 22, 2013

   dx.doi.org/10.1021/ic3027094 | *Inorg. Chem.* 2013, 52, 4458−4463

Titanium sesquioxide, Ti_2O_3, attracts attention by a second-order semiconductor-to-metal transition upon heating.[17] Numerous studies were carried out to understand this behavior. The most widely accepted model for the Ti_2O_3 semiconductor-to-metal transition involves a band-crossing mechanism.[18] The crystal structure of this oxide contains two different kinds of Ti−Ti distances.[14] One of them corresponds to a sum of the covalent radii of titanium (2.99 Å), whereas the second one is significantly shorter (2.58 Å), which may indicate a strong cation−cation interaction.[18] The theoretical calculation predicts that this short Ti−Ti distance is required to open a semiconducting gap.[19] This suggests that electron−electron correlation effects may provide the key for understanding the semiconductor-to-metal transition in Ti_2O_3. The changes in the structural parameters of Ti_2O_3 occur in the temperature range 373−573 K. In the same range, Ti_2O_3 shows a 50-fold drop in resistivity,[20] a specific heat anomaly,[21] as well as significant changes in the elastic constants,[22] the magnetic susceptibility,[23] and the Raman spectrum.[24] The changes of the short Ti−Ti distances are very sensitive to temperature, and their behavior is nonlinear in the same temperature ranges,[25] which cannot be explained solely on the basis of normal thermal expansion.

Further work was devoted to the thermoelectric/transport properties of Ti_2O_3.[26,27] Experimentally, bulk Ti_2O_3 has been found to be a semiconductor below 450 K with a rather small band gap of ≈0.1 eV.[28] However, early attempts to reproduce this gap using theoretical tools have been unsuccessful.[18] Recently, using cluster dynamical-mean-field theory, it was shown that the semiconductor-to-metal transition can successfully be reproduced for Ti_2O_3.[28] Nonetheless, the complete picture of the electrical and thermal transport behavior of titanium sesquioxide is still under investigation. From the chemical point of view, it is worth mentioning that even the color of the compound was described differently: from black,[29a] black blue,[29b] to (dark) violet,[30] which may indicate the presence of the Magnéli phases with titanium in mixed or intermediate valence states in the samples.

In this work, we present a novel preparation route based on the SPS technique for the synthesis and shaping of bulk Ti_2O_3 in a single step. Chemical characterization and thermoelectric properties of the SPS-synthesized Ti_2O_3 are discussed.

Synthesis. Powders of rutile (99.8 mass %, Alfa Aesar) or anatase (99.6 mass %, Alfa Aesar) and titanium (99.9 mass %, Alfa Aesar) were used. SPS experiments were carried out utilizing a SPS-515 ET, Dr. Sinter setup [Fuji SDC (SPS Syntex), Japan]. The mixtures of powders were prepared in an argon-filled glovebox and loaded into graphite dies of inner diameter of 8 mm. Carbon foil was used to separate the powder specimen from the graphite die and punches. Successful preparation was achieved by heating to 1473 K with a rate of 50 K min^{-1} under a uniaxial pressure of 60 MPa in a vacuum (≤10 Pa), holding at these conditions for 180 min, and then cooling to room temperature. The temperature measurement within the SPS setup is performed either by means of a thermocouple inside the die wall (in the temperature region below 1073 K) or by a pyrometer on the surface of the die (in the high-temperature region 850−2270 K). To minimize thermal radiation, the die was wrapped with graphite fleece.

Characterization. Finely ground powders were fixed with vacuum grease (Lithelen, Leybold) on a polyimide film (d = 5 μm, Chemplex). Powder X-ray diffraction (PXRD) patterns were measured on a Huber G670 camera (Guinier geometry, Cu Kα_1 radiation, λ = 1.540562 Å, graphite monochromator, 5° ≤ 2θ ≤ 100°, and $\Delta 2\theta$ = 0.005°). Data evaluation was made by means of *WinXPow* software.[31] The positions of the reflections were determined by a single profile fit with LaB_6 as the internal standard [NIST; a = 4.1569162(97) Å at 295.5 K]. The lattice parameters were obtained from a least-squares refinement with the program package *WinCSD*.[32]

For their metallographic characterization, the SPS specimens were cut perpendicularly to the pressure direction exerted within the SPS treatment. The surface area was prepared by SiC grinding and vibration polishing (VibroMet 2, Buehler) with a 0.05 μm Al_2O_3 slurry. The microstructures were studied by optical microscopy (Axioplan2, Zeiss) as well as energy-dispersive X-ray spectroscopy performed on a scanning electron microscope [Philips XL30 LaB_6; EDAX Pheonix system, Si(Li) detector]. Carbon-coated specimens have been used for scanning electron microscopy analysis.

Electrical resistivity and thermopower were measured simultaneously using a commercial setup (ZEM-3, Ulvac-Riko) in the temperature range 300−800 K. Specific heat measurements were conducted on a Netzsch Pegasus differential scanning calorimeter. For these measurements, the specimens were heated up to 1073 K under an argon atmosphere with a heating rate of 10 K min^{-1}. The thermal diffusivity α was measured by means of a laser-flash apparatus (Netzsch LFA 457). The total thermal conductivity was subsequently calculated by $\kappa = \alpha C_p \rho_V$, where C_p and ρ_V are the specific heat capacity and density, respectively.

RESULTS AND DISCUSSION

The previously found preparation routes for Ti_2O_3 are reduction of titanium dioxide by hydrogen at 1000 °C or by elemental titanium at 1600 °C. So far, Ti_2O_3 and other titanium oxides were obtained from TiO_2 and titanium either by arc-melting[11] and subsequent annealing or by oxidizing TiO.[26] The drawback of both synthesis methods is the difficulty in controlling the reaction progress at elevated temperatures and the homogeneity of the final product.[30] In order to overcome the latter, the intermediate mixtures have to be reground and rereacted, finally yielding powder products. This hinders the measurements of the transport properties. Thus, single-crystal growth was necessary to obtain single-phase specimens for the property investigations. The single crystals were grown by the Czochralski method.[14]

Here, the SPS technique was applied for the simultaneous synthesis, densification, and shaping of Ti_2O_3. This kind of treatment was applied earlier, in particular, for a low-temperature synthesis and densification of skutterudite derivatives $CoSb_3$ and $LaFe_4Sb_{12}$,[33] as well as intermetallic compounds TiB_2,[34] Ti_5Si_3,[35] Mg_2Si,[36] and MgB_2.[37] These materials were obtained from mixtures of the elements or from precursors. Such solid-state reactions are based on the mass transport of reagents within the powder mixture.[38] From the chemical point of view, these SPS preparations are redox reactions. This was clearly shown by recent studies of the SPS preparation of $Na_{24}Si_{136}$ from Na_4Si_4. At the cathode, silicon anions were oxidized to Si^0, whereas the anode served to reduce sodium cations to an elemental metal.[39]

All samples with the nominal final composition Ti_2O_3 investigated in this work were synthesized in a single-step reactions starting from the mixtures of powders of rutile/anatase and metallic titanium in a molar ratio of 3:1 according to the reaction $3TiO_2 + Ti = 2Ti_2O_3$. The reaction conditions and results for selected samples are summarized in Table 1.

dx.doi.org/10.1021/ic3027094 | *Inorg. Chem.* 2013, 52, 4458−4463

Table 1. Reaction Temperature and Products of SPS-Prepared Ti_2O_3 Samples

T, K	products
	Anatase as the starting component
873	anatase + rutile + Ti
1073	rutile + TiO_{2-x} + Ti_3O
1273	Ti_2O_3 + Ti_3O_5 + Ti_4O_5 + Magnéli phases (traces)
	Rutile as the starting component
873	rutile + Ti
1073	rutile + TiO_{2-x} + Ti_3O
1273	Ti_2O_3 + Ti_3O_5 + Ti_4O_5 + Magnéli phases (traces)
1473	Ti_2O_3

At temperatures between 820 K and 1270 K, anatase transforms into the equilibrium rutile phase.[40] Indeed, the presence of rutile was observed in the PXRD pattern of a sample obtained at 873 K from anatase and titanium. No chemical reactions between the starting components were found below 873 K. The samples have a white color with black metallic inclusions. The anatase-to-rutile transformation was found to be completed at 1073 K. The PXRD patterns of samples with anatase and rutile as starting materials obtained at temperatures above 1073 K are identical. Thus, further considerations will deal exemplarily only with those samples for which rutile was used as a starting component. The first changes visible in the PXRD patterns were observed for the samples that were SPS-treated at 1073 K (Figure 1a). Besides

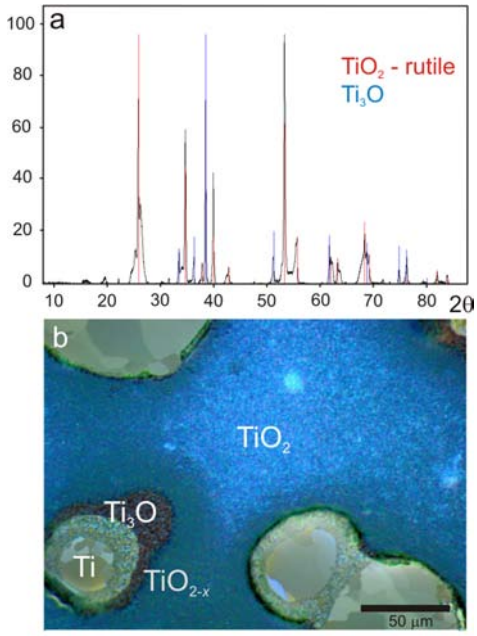

Figure 1. Products of the SPS reaction of rutile and titanium at 1073 K: (a) PXRD pattern showing reflections of TiO_{2-x} and Ti_3O along with those of rutile; (b) microstructure exhibiting a distribution of spherical titanium particles (light blue) in an oxide matrix (blue).

the main-phase rutile, partially decomposed TiO_{2-x} and titanium-rich phase Ti_xO (Ti_3O) are detected. It is clearly seen from the microstructure (Figure 1b) that titanium particles act as reaction centers and are surrounded by layers of titanium-rich suboxide Ti_3O and of oxygen-deficient TiO_{2-x}. All of these phases are embedded in the rutile matrix.

The reaction continues when the temperature is increased. As a result, the SPS-treated sample at 1273 K contains Ti_2O_3 and Ti_3O_5 in equal amounts, some Ti_4O_5, and traces of other Magnéli phases (Figure 2a). The latter are difficult to identify

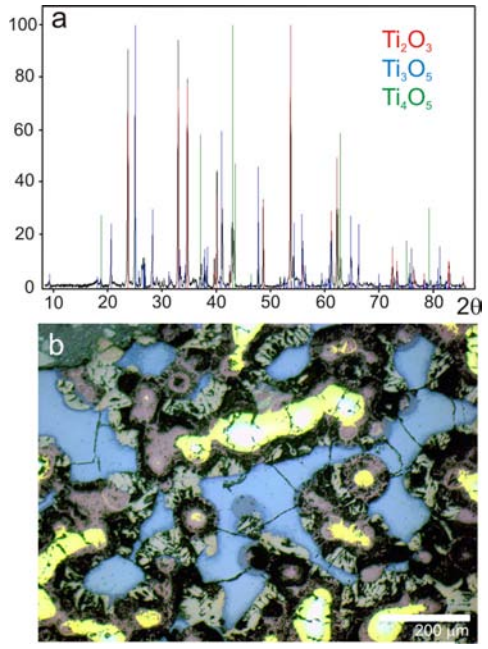

Figure 2. Products of the SPS reaction of rutile and titanium at 1273 K: (a) PXRD pattern showing reflections of Ti_2O_3, Ti_3O_5, Ti_4O_5, and traces of other Magnéli phases; (b) microstructure exhibiting a distribution of six different phases.

more precisely because of the weak intensities of most of the reflections and complex diffraction pattern of these phases. The microstructure reveals at least six phases, which are spatially arranged in a complex manner (Figure 2b). Titanium-rich phases, and also residues of initial titanium, are surrounded by oxygen-enriched areas. The phases Ti_4O_5 and Ti_3O_5 are closer in composition to Ti_2O_3 compared with Ti_3O and TiO_{2-x}.

Finally, Ti_2O_3 as a single phase was obtained at 1473 K after 180 min of SPS treatment (Figure 3). Contrary to the descriptions made in some previous publications, the color of the compound is light brown. In combination with the metallographic investigation of the microstructure, this proves the absence of impurities with the mixed or intermediate valence of titanium, e.g., Magnéli phases. The geometrical density was found to be 95% of the value calculated from the crystal structure.

From the experimental findings, the following reaction scenario may be proposed. The components of the starting mixture (TiO_2 and titanium) react at the contact surface only. At first, those phases form compositions that differ only slightly from the compositions of the starting materials (Ti_3O and TiO_{2-x} at 1073 K). After longer SPS treatment or after a treatment at increased temperature, further Ti−O phases with compositions closer to Ti_2O_3 are formed by diffusion; i.e., the distribution of titanium and oxygen in the sample becomes more homogeneous. Finally, only the target phase Ti_2O_3 is observed. Formation of the Ti_2O_3 phase is therefore a diffusion-controlled reaction.

Crystal Structure. All observed reflections in the PXRD pattern (Figure 3a) could be indexed assuming a rhombohedral

dx.doi.org/10.1021/ic3027094 | Inorg. Chem. 2013, 52, 4458−4463

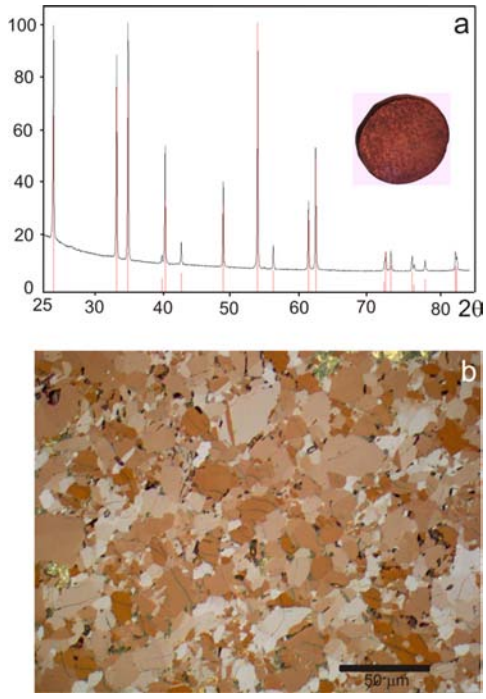

Figure 3. Product of the SPS reaction of rutile and titanium at 1473 K: (a) PXRD pattern showing reflections of Ti_2O_3; (b) microstructure exhibiting a distribution of one Ti_2O_3 phase (black areas correspond to voids/holes in the sample).

lattice with lattice parameters a = 5.1586(1) Å and c = 13.6040(1) Å (structure type α-Al_2O_3, space group $R\bar{3}c$). A narrow homogeneity range of Ti_2O_3 with a slight variation of the lattice parameters between a = 5.160 Å and c = 13.60 Å for $Ti_2O_{2.98}$ and a = 5.147 Å and c = 13.64 Å for $Ti_2O_{3.02}$ was reported earlier.[11] Considering this homogeneity range, the observed lattice parameters indicate a slight oxygen deficiency of our product.

The crystal structure of Ti_2O_3 belongs to the α-Al_2O_3 (corundum) type and can be understood as a hexagonal close packing of oxygen atoms, with trivalent titanium cations inside the octahedral cavities (Figure 4).[11,14] Along the 3-fold axis,

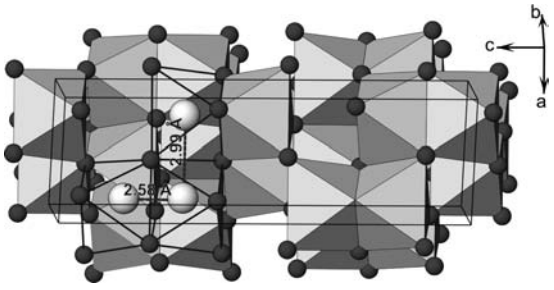

Figure 4. Crystal structure of Ti_2O_3. Black spheres − oxygen, titanium atoms are located within the octahedrons and are only exemplarily shown by gray spheres.

titanium cations occupy octahedra that share common faces between edges within layers. The shortest cation−cation distance of 2.58 Å is formed between the layers; the longer one of 2.99 Å is observed within layers. The interlayer Ti−Ti interaction may be a key for the interesting electrical and heat transport. In addition, the crystal-chemical behavior of Ti^{3+} species allows for a partial substitution by other transition metals and, thus, opens the way to modifying physical properties.

Thermoelectric Properties. The semiconductor-to-metal transition observed in Ti_2O_3 manifests itself in a peak of the temperature-dependent specific heat at 450 K for the SPS-treated sample at 1473 K (Figure 5).

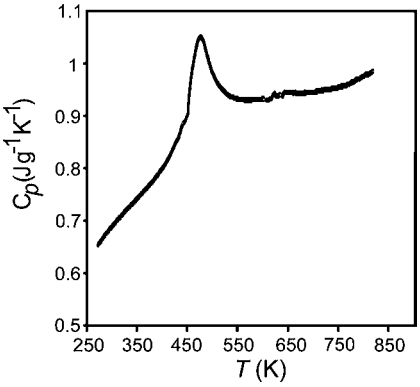

Figure 5. Temperature dependence of the specific heat C_p of Ti_2O_3.

During this transition, the resistivity ρ drops by about 2 orders of magnitude for the single-phase Ti_2O_3 (Figure 6a). Above the transition temperature, the slope $\rho(T)$ resembles a bad-metal behavior (Figure 6a). Below the transition temperature, the thermopower α is positive (Figure 6b). Above 400 K, the thermopower changed sign toward negative values but is much less temperature-dependent (Figure 6b) compared to that of rutile and, thus, is in agreement with the higher electrical conductivity of Ti_2O_3 in this temperature region. These results are in well agreement with the literature data in the investigated temperature range (resistivity change from 1×10^{-2} Ω cm at 300 K to 1×10^{-4} Ω cm at 800 K[20] and thermopower change from 180 μV K^{-1} at 300 K to −10 μV K^{-1} at 800 K[15]). The observed behavior is well in agreement with the electronic structure calculations.[28]

The thermal conductivity $\kappa(T)$ of Ti_2O_3 falls within the range of 3 and 5 W m^{-1} K^{-1} (Figure 6c). It decreases upon approaching the transition temperature, as expected for an insulator, and increases slightly again at temperatures above the transition temperature, a behavior that is in agreement with the electronic conductivity (cf. the thermopower).

The thermoelectric figure-of-merit for Ti_2O_3 (Figure 6d) is low in the investigated temperature range. Below the transition temperature, it increases slightly with temperature, dropping close to zero at elevated temperatures because of a strongly increased electrical conductivity. The influence of chemical substitutions on the thermoelectric properties of Ti_2O_3 is the focus of an ongoing study.

■ CONCLUSIONS

Dense specimens of Ti_2O_3 with given shape were synthesized in pursuing a new preparation route. This route consists of a single-step reaction starting from powder mixtures of rutile/anatase and metallic titanium using the SPS technique. Ti_2O_3 as a single phase was obtained at 1473 K after 180 min of SPS treatment. The electronic and thermal transport properties reflect a transition from semiconductor to metallic behavior above 400 K. The observed metallic-like behavior above this temperature is in good agreement with previously reported

dx.doi.org/10.1021/ic3027094 | Inorg. Chem. 2013, 52, 4458−4463

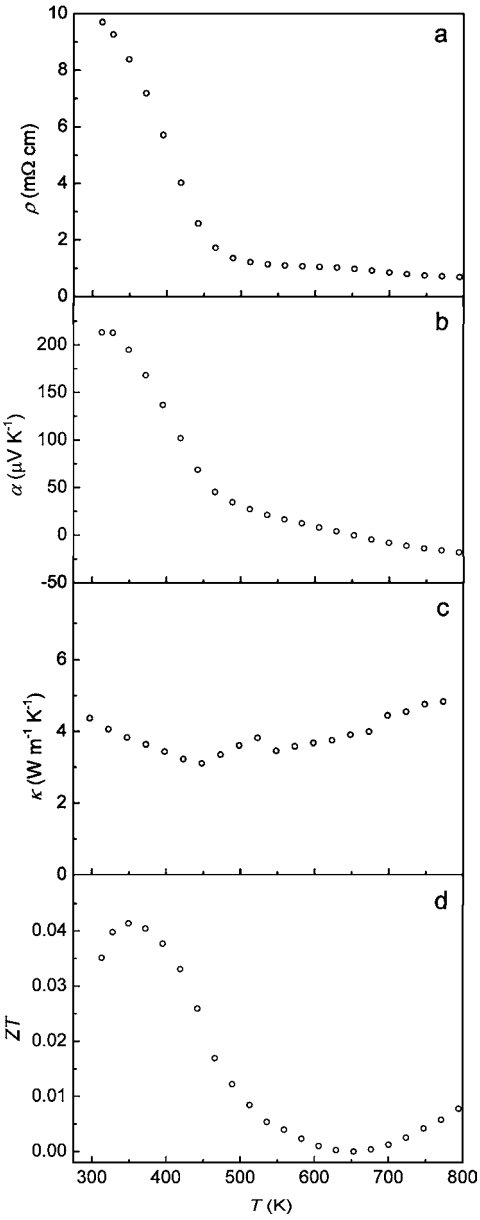

Figure 6. Temperature dependence of the electrical resistivity ρ (a), the thermopower α (b), the thermal conductivity κ (c), and the dimensionless figure-of-merit ZT (d) for Ti_2O_3.

results. The figure-of-merit is low: a maximum ZT of 0.04 is achieved at 350 K.

AUTHOR INFORMATION

Corresponding Author

*E-mail: Igor.Veremchuk@cpfs.mpg.de.

Author Contributions

The work was made in cooperation between two research groups. The manuscript was written through contributions of all authors. All authors have given approval to the final version of the manuscript.

Funding

I.V. and Y.G. acknowledge financial support within the ECEMP at TU Dresden (Project B3), which was funded by the European Union (EFRE) and the Free State of Saxony.

Notes

The authors declare no competing financial interest.

ACKNOWLEDGMENTS

The authors thank S. Kostmann for metallographic preparations and the competence group 'Structure' at MPI CPfS for the X-ray diffraction experiments.

REFERENCES

(1) Tokita, M. *J. Soc. Powder Technol. Jpn.* **1993**, *30*, 790.
(2) Orrù, R.; Licheri, R.; Locci, A. M.; Cincotti, A.; Cao, G. *Mater. Sci. Eng. R* **2009**, *63*, 127.
(3) Ohtaki, M.; Ogura, D.; Eguchi, K.; Arai, H. *J. Mater. Chem.* **1994**, *4*, 653.
(4) Ohtaki, M.; Koga, H.; Tokunaga, T.; Eguchi, K.; Arai, H. *J. Solid State Chem.* **1995**, *120*, 105. Flahaut, D.; Mihara, T.; Funahashi, R.; Nabeshima, N.; Lee, K.; Ohta, H.; Koumoto, K. *J. Appl. Phys.* **2006**, *100*, 084911. Huang, X. Y.; Miyazaki, Y.; Kajitani, T. *Solid State Commun.* **2008**, *145*, 132.
(5) Muta, H.; Kurosaki, K.; Yamanaka, S. *J. Alloys Compd.* **2003**, *350*, 292. Obara, H.; Yamamoto, A.; Lee, C.-H.; Kobayashi, K.; Matsumoto, A.; Funahashi, R. *Jpn. J. Appl. Phys.* **2004**, *43*, L540. Okuda, T.; Nakanishi, N.; Miyasaka, S.; Tokura, Y. *Phys. Rev. B* **2001**, *63*, 113104. Ohta, S.; Nomura, T.; Ohta, H.; Koumoto, K. *J. Appl. Phys.* **2005**, *97*, 034106. Ohta, S.; Nomura, T.; Ohta, H.; Hirano, M.; Hosono, H.; Koumoto, K. *Appl. Phys. Lett.* **2005**, *87*, 092108. Ohta, S.; Ohta, H.; Koumoto, K. *J. Ceram. Soc. Jpn.* **2006**, *114*, 102.
(6) Ohta, H.; Seo, W. S.; Koumoto, K. *J. Am. Ceram. Soc.* **1996**, *79*, 2193. Kazeoka, M.; Hiramatsu, H.; Seo, W.-S.; Koumoto, K. *J. Mater. Res.* **1998**, *13*, 523. Kaga, H.; Asahi, R.; Tani, T. *Jpn. J. Appl. Phys.* **2004**, *43*, 7133.
(7) Ohtaki, M.; Tsubota, T.; Eguchi, K.; Arai, H. *J. Appl. Phys.* **1996**, *79*, 1816. Tsubota, T.; Ohtaki, M.; Eguchi, K.; Arai, H. *J. Mater. Chem.* **1997**, *7*, 85. Tsubota, T.; Ohtaki, M.; Eguchi, K.; Arai, H. *J. Mater. Chem.* **1998**, *8*, 409.
(8) Terasaki, I.; Sasago, Y.; Uchinokura, K. *Phys. Rev. B* **1997**, *56*, R12685. Maeda, E.; Ohtaki, M. *Trans. Mater. Res. Soc. Jpn.* **2000**, *25*, 237. Ito, M.; Nagira, T.; Furumoto, D.; Katsuyama, S.; Nagai, H. *Scr. Mater.* **2003**, *48*, 403.
(9) Funahashi, R.; Matsubara, I.; Ikuta, H.; Takeuchi, T.; Mizutani, U.; Sodeoka, S. *Jpn. J. Appl. Phys.* **2000**, *39*, L1127. Wang, D.; Cheng, L.; Yao, Q.; Li, J. *Solid State Commun.* **2004**, *129*, 615.
(10) Funahashi, R.; Shikano, M. *Appl. Phys. Lett.* **2002**, *81*, 1459.
(11) Andersson, S.; Collén, B.; Kuylenstierna, U.; Magnéli, A. *Acta Chem. Scand.* **1957**, *11*, 1641.
(12) *Binary Alloy Phase Diagrams*, 2nd ed.; Massalski, T.B., Ed.; ASM International: Materials Park, OH, 1990; Vol. 3, pp 2924−2927.
(13) Le Page, Y.; Strobel, P. *J. Solid State Chem.* **1982**, *44*, 273.
(14) Vincent, M. G.; Yvon, K.; Grüttner, A. *Acta Crysallogr.* **1980**, *A36*, 803.
(15) Harada, Sh.; Tanaka, K.; Inui, H. *J. Appl. Phys.* **2010**, *108*, 083703.
(16) Okinaka, N.; Akiyama, T. *Jpn. J. Appl. Phys.* **2006**, *45*, 7009.
(17) Naylor, B. I. *J. Am. Chem. Soc.* **1946**, *68*, 1077.
(18) Goodenough, J. B. *Phys. Rev.* **1960**, *117*, 1442.
(19) Mattheiss, L. F. *J. Phys.: Condens. Mater.* **1996**, *8*, 5987.
(20) Honig, J. M.; Reed, T. B. *Phys. Rev.* **1968**, *174*, 1020.
(21) Barros, H. L.; Chandrashekhar, G. V.; Chi, T. C.; Honxg, J. M.; Sladek, R. J. *Phys. Rev. B* **1973**, *7*, 5147.
(22) Chi, T. C.; Sladek, R. J. *Phys. Rev. B* **1973**, *7*, 5080.
(23) Pearson, A. D. *J. Phys. Chem. Solids* **1958**, *5*, 316.
(24) Moordian, A.; Raccah, P. M. *Phys. Rev. B* **1971**, *3*, 4253.
(25) Rice, C. E.; Robinson, W. R. *Acta Crystallogr., Sect. B* **1977**, *33*, 1342.
(26) He, Q.; Hao, Q.; Chen, G.; Poudel, B.; Wang, X.; Wang, D.; Ren, Z. *Appl. Phys. Lett.* **2007**, *91*, 052505.
(27) Afifi, M. A.; Abdel-Aziz, M. M.; Yahia, I. S.; Fadel, M.; Wahab, L. A. *J. Alloys Compd.* **2008**, *455*, 92.

(28) Poteryaev, A. I.; Lichtenstein, A. I.; Kotliar, G. *Phys. Rev. Lett.* **2004**, *93*, 086401−1.
(29) (a) Wiberg, N. *Holeman−Wiberg Lehrbuch der Anorganischen Chemie*, 101st ed.; Walter de Gruyter: Berlin, 1995; p 1404. (b) Wiberg, N. *Holeman−Wiberg Lehrbuch der Anorganischen Chemie*, 101st ed.; Walter de Gruyter: Berlin, 1995; p 1408.
(30) Brauer, G. *Handbuch der Präparativen Anorganischen Chemie*; Enke : Stuttgart, Germany, 1963; Vol. *2*, pp 1364−1366.
(31) *WinXPow*, version 2.08; STOE and Cie GmbH: Darmstadt, Germany, 2003.
(32) Akselrud, L. G.; Zavalii, P. Yu.; Grin, Yu.; Pecharsky, V. K.; Baumgartner, B.; Wölfel, E. *Mater. Sci. Forum* **1993**, *133−136*, 335.
(33) Recknagel, C.; Reinfried, N.; Höhn, P.; Schnelle, W.; Rosner, H.; Grin, Yu.; Leithe-Jasper, A. *Sci. Technol. Adv. Mater.* **2007**, *8*, 357.
(34) Schmidt, J.; Boehling, M.; Burkhardt, U.; Grin, Yu. *Sci. Technol. Adv. Mater.* **2007**, *8*, 376.
(35) Handtrack, D.; Despang, F.; Sauer, C.; Kieback, B.; Reinfried, N.; Grin, Yu. *Mater. Sci. Eng., A* **2006**, *437*, 423.
(36) Schmidt, M.; Schmidt, J.; Grin, Yu.; Böhm, A.; Kieback, B.; Scholl, R.; Schubert, Th.; Weissgärber, Th.; Zumdick, M. Int. Patent PCT/EP02/03953, Sept 4, 2002.
(37) Schmidt, J.; Grin, Yu. Int. Patent PCT/EP02/03952, Sept 4, 2002.
(38) Munir, Z. A.; Anselmi-Tamburini, U.; Ohyanagi, M. *J. Mater. Sci.* **2006**, *41*, 763.
(39) Beekman, M.; Baitinger, M.; Borrmann, H.; Schnelle, W.; Meier, K.; Nolas, G. S.; Grin, Yu. *J. Am. Chem. Soc.* **2009**, *131*, 9642.
(40) Hanaor, D.; Sorrell, C. *J. Mater. Sci.* **2011**, *437*, 1.